9-15-2014

A Paper-Based Calorimetric Microfluidics Platform for Biochemical Sensing

Benyamin Davaji
Marquette University

Chung Hoon Lee
Marquette University, chunghoon.lee@marquette.edu

Biosensors and Bioelectronics, Vol. 59 (September 15, 2014): 120-126. DOI.

A Paper-based Calorimetric Microfluidics Platform for Bio-chemical Sensing

Benyamin Davaji
Nanoscale Devices Laboratory, Marquette University, Milwaukee, WI
Chung Hoon Lee
Nanoscale Devices Laboratory, Marquette University, Milwaukee, WI

Abstract

In this report, a paper-based micro-calorimetric biochemical detection method is presented. Calorimetric detection of biochemical reactions is demonstrated as an extension of current colorimetric and electrochemical detection mechanisms of paper-based biochemical analytical systems. Reaction and/or binding temperature of glucose/glucose oxidase, DNA/hydrogen peroxide, and biotin/streptavidin, are measured by the paper-based micro-calorimeter. Commercially available glucose calibration samples of 0.05, 0.15 and 0.3% wt/vol concentration are used for comparing the device performance with a commercially available glucose meter (electrochemical detection). The calorimetric glucose detection demonstrates a measurement error less than 2%. The calorimetric detection results of DNA concentrations from 0.9 to 7.3 mg/mL and temperature changes

in biotin and streptavidin reaction are presented to demonstrate the feasibility of integrating the calorimetric detection method with paper based microfluidic devices.

Keywords
Micro-calorimetry, Thermal bio-sensor, Label-free detection, Paper-based sensor

1. Introduction
The first paper-based chemical analytical technique was chromatography and was developed by Martin and Synge (Martin, 1952) in 1943. The first immunoassay using paper as a fluidic channel was reported by Muller (Muller and Clegg, 1949). More recently, paper-based microfluidics were re-introduced by Martinez et al. (2007) for low-cost disposable bio-chemical sensing applications. Further development and extension of this technique for higher accuracy and extended functionality were demonstrated recently using microfabricated devices (Liana et al., 2012, Martinez et al., 2008b). Inexpensive paper-based microfluidic systems have also been expanded to other applications such as environmental monitoring (Liana et al., 2012, Li et al., 2012). Paper-based microfluidic devices exploit capillary action in porous paper to transport and manipulate liquid samples. This extremely simple and robust liquid transport mechanism is well-suited for the development of assays, particularly in applications where portability and/or disposability are important. As a result, paper-based analytical techniques are used in several commercially available products such as glucose-meter strips, pregnancy test strips, and pH strips.

Biochemical assays have been developed and commercialized based on several different types of detection methods. The most popular detection methods are colorimetric (Ellerbee et al., 2009, Martinez et al., 2008a) and electrochemical (Nie et al., 2010, Dungchai et al., 2011). Colorimetric detection is based on changes in intensity of colors due to the reaction of a reagent and a sample. The changes in color (wavelength) and intensity can be detected using a camera, spectroscopy, or in some applications, even by the unaided human eye. Electrochemical detection is based on changing electroinactive substrates to electroactive products (Wang, 2008). In the electrochemical detection readout is an electrical signal representing the change in electrical conductivity or electrical potential providing a quantification of the chemical reaction. Colorimetric detection has been widely used for inexpensive semi-quantitative assays to indicate the presence or absence of targeted molecules. However, precise quantification of the chemical reaction typically requires complex optical detection instrumentation (Ellerbee et al., 2009) or image processing software (Martinez et al., 2008a), which is not suitable for the development of inexpensive portable devices. An added difficulty is the requirement to develop dyes that change color or intensity via a reaction with the molecule being measured. Electrochemical detection systems are easier to miniaturize because they only need to quantify electrical conductivity or changes in potential. However, this technique requires reactions that produce electroactive molecules.

In this paper, a calorimetric paper-based microfluidic system for bio-chemical sensing is presented for the first time. Since most bio-chemical reactions or interactions are accompanied by a change in heat, this label free calorimetric detection method extends and enhances the capabilities of existing paper-based microfluidic systems to include a wide range of bio-chemical sensing and diagnostic applications.

2. Materials and methods
2.1. Micro-calorimetric detection
Thermal detection methods have been used by others to explore bio-chemical interactions (Allen and Lai, 1998, Abramson and Tien, 1999, Yi et al., 2014, Kwak et al., 2008). In this method, the temperature changes resulting from endothermic or exothermic reactions are used to detect and/or quantify the concentrations of

targeted molecules. However, it is impractical to use a traditional macro-scale calorimeter for disposable and inexpensive sensing applications. A paper-based microcalorimetric device, as shown in Fig. 1(a), offers a number of advantages: small volume of required sample, ease of sample handling, increased sensitivity at micro-scale, and low-cost manufacturing.

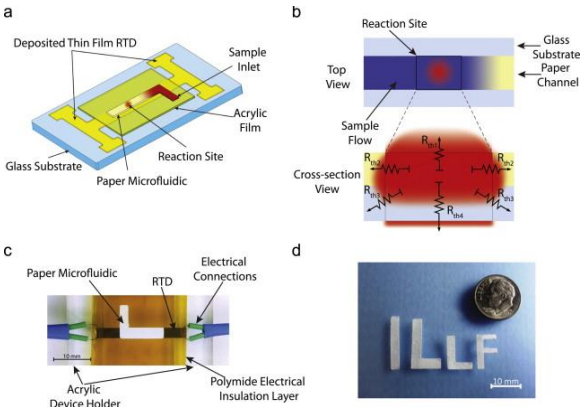

Fig. 1. (a) Overview of the paper-based device, (b) top view and cross-sectional view of the reaction site and heat transfer with the thermal resistance equivalent model, (c) fabricated paper-based microfluidic device with calorimetric detection, (d) knife plotter cut paper strips as a reaction substrate and a microfluidic channel.

The heat generated or absorbed from a bio-chemical reaction causes a temperature change, which depends on the concentration of the reagent and the samples and the enthalpy of the reaction. It can be readily shown that the sensitivity of the temperature detection of a calorimeter is inversely proportional to its heat capacity (Barnes et al., 1994, Lai et al., 1995).

From generated heat in reaction the temperature change can be expressed by

(1) $\Delta T = (1/C_p)\Delta Q$

where *T* is the temperature, *Q* is the heat, and C_p is the heat capacity.

A paper-based microfluidic system has the inherent advantage of a low thermal mass due to the thin and porous nature of the paper and thin glass substrate configuration as shown in Fig. 1(a). In order to measure the temperature changes from the reaction, the measurement system is ideally required to be in the adiabatic condition. The adiabatic condition ensures that all of the heat released or absorbed from the reaction is used to affect a temperature change, rather than lost to the surroundings before the temperature change is measured. However, with practical calorimeters it is only possible to achieve a quasi-adiabatic condition. The amount of heat lost to the surroundings can be characterized by a thermal time constant, which is a function of the heat capacity of the calorimeter and the thermal resistance between the calorimeter and its surroundings (i.e., its thermal isolation). Fig. 1(b) shows a schematic cross-sectional view of the sensor where the chemical reaction occurs in the spot indicated in the figure. Fig. 1(b) shows the lumped equivalent circuit model representing the thermal conductivity from the reaction area. Using a first order approximation, the thermal time constant of the system can be expressed as

(2) $\tau = R_{th}C_p$

where R_{th} is the thermal resistance and C_p is the thermal capacity of the system, respectively.

The R_{th} can be calculated as

(3) $R_{th} = L/(kA)$

for a material bounded surface and

(4) $R_{th} = 1/(4kr)$

for an air bounded surface (Carslaw and Jaeger, 1986), where *L* is the length along the heat flow direction, *k* is the thermal conductivity of material, *A* is the area perpendicular to the heat flow, and *r* is the radius of area. The total thermal resistance of our system can be expressed as

(5) $R_{th} = R_{th1} \parallel R_{th2} \parallel R_{th2} \parallel R_{th3} \parallel R_{th3} \parallel R_{th4}$

where the R_{th1} to R_{th4} are the thermal resistances for each of the components indicated in Fig. 1(b).

The total heat capacity can be expressed as

(6) $C_p = C_{pg} + C_{pp\text{ł}}$

where C_{pg} is the heat capacity of the glass substrate and $C_{pp\text{ł}}$ is the heat capacity of the paper and liquid. The heat capacity can be expressed as

(7) $C_p = \rho V c_p$

where ρ is the mass density of the material, *V* is the volume and C_p is the constant volume specific heat of the material.

Table 1 lists the thermal parameters of a micro-calorimeter of typical dimensions used in this work. In this case, the micro-calorimeter was made of a 100µm thick glass substrate and a 180µm thick paper microfluidic channel. The reagent was immobilized within a 3×4 mm area of the channel, called the reaction site. It was assumed that the reaction within the reaction site is homogeneous and that the reaction is not diffusion-limited. Thus the reaction site in this device was considered to be isothermal. In Table 1, $C_{p,Calc}$ is the calculated thermal mass of the system, $C_{p,M}$ is the measured thermal mass of device, τ_{Calc} and τ_{M} are the calculated and measured time constants, respectively. The calculated heat capacity is in close agreement with the measured heat capacity as discussed later.

Table 1. Thermal parameters of the device.

Symbol	Parameter	Unit	Value
R_{th1}	R_{th} of air boundary	K/W	6.17×10^{3}
R_{th2}	R_{th} of paper boundary	K/W	4.78×10^{3}
R_{th3}	R_{th} of glass boundary	K/W	4.76×10^{3}
R_{th4}	R_{th} of air through glass	K/W	6.17×10^{3}
$C_{\mathrm{P,Calc.}}$	Calculated thermal mass	J/K	1.33×10^{-2}
$C_{p,M}$	Measured thermal mass	J/K	1.42×10^{-2}
$\tau_{Calc}.$	Calculated time constant	s	11.3
τ_{M}	Measured time constant	s	12.4

The paper-based microcalorimeter presented here is bounded by air on the top of the device, which has a high thermal resistivity. However, convection of air can be a significant thermal path for most thermal measurements. To suppress the convection of air, an enclosure can be used. Radiation is also a thermal loss pathway, but it is significant only at high temperature differences between the system and its surroundings (Bergman et al., 2011). Radiation losses in paper-based microfluidic systems are neglected because most bio-chemical reactions result in lower temperature differences than those required for significant radiation loss.

2.2. Paper-based thermal calorimeter platform

The paper-based device consisted of a microfluidic channel made of a chromatography-grade filter paper placed directly on top of a resistive temperature detector (RTD), as shown in Fig. 1(c). A 100µm thick cover glass (VWR 48393-106) was used as a substrate for the paper and RTD. A thin layer of 5µm acrylic film (Nitto Denko 5600) was used for electrical isolation and also served as the adhesion layer between the paper microfluidic channel and the glass substrate.

2.2.1. Microfluidic channel design

The mechanism of liquid transport by capillary action simplifies microfluidic systems by eliminating the need for actuation (pumping) and valves to control the flow. An important advantage of this technique is bubble-free operation. Suppressing or preventing bubble formation in microfluidic devices has long been a challenge during sample introduction and operation (Cho et al., 2007, Sung and Shuler, 2009), but is necessary to produce reliable and repeatable results.

The material of the reaction site (paper microfluidic channel) plays a key role in enzyme-based detection of bio-chemical reactions. Various reaction substrates (e.g. cellulose, solid glass particles, porous glass particles, and nickel screen) have been used for immobilizing glucose oxidase (GOD) enzyme. Among these, porous glass and cellulose fiber networks are the most common materials due to their high surface area (Bankar et al., 2009).

In our design chromatography filter paper (Whatman3001-845) was used as a microfluidic channel and a reagent substrate. Laser cutting has been used to cut paper strips to make the microfluidic channel (Fu et al., 2011) but the residue of burned paper along the cutting line will remain on the paper which may interfere with the reaction. Our paper fluidic channel was patterned and cut using a knife plotter (from Silhouette, Inc.). The patterns were designed to guide the sample flows in the paper strip. The paper strip was affixed on top of the RTD, which was integrated on the glass substrate. In order to minimize the mechanical stress caused by introducing liquids to the RTD, L- and F-shaped designs were used instead of a straight strips. Examples of the paper fluidic channels cut by the knife plotter are shown in Fig. 1(d). The tails of the L-shape and F-shape papers were positioned outside the RTD, where the samples were introduced. In this paper, the L-shape design was used to obtain a simpler geometry (increasing uniformity of enzyme distribution on paper) for an enzyme immobilization site. In each measurement, a known amount of reagent was placed at the center of the channel. The introduced sample was transported by capillary action towards the reagent. Once the sample came in contact with the reagent, the reaction started.

In previous works, paper-based fluidic channels were fabricated by using wax printing (Carrilho et al., 2009, Martinez et al., 2008b) and photolithography (Martinez et al., 2007). In this work, a knife plotter tool was used to cut out precise paper microchannels. The knife plotter method also results in minimal chemical contamination of the paper and requires no heat treatment, which prevents the cellulose network from developing defects and eliminates solvent diffusion into the paper. Paper strips defined by the knife plotter also provide a higher integration capability for 3D microfluidics to define more complex shapes (Liu and Crooks, 2011).

2.2.2. RTD design, fabrication and measurement

A resistive temperature detector (RTD) was used to detect the temperature change in the reaction and is preferred over other temperature sensors due to its excellent linearity, high sensitivity, low fabrication cost, easy integration, and simple readout and interfacing. Typically, platinum is used for commercial RTD sensors due to its chemical inertness and linearity of resistance change over wide temperature ranges (−50 to 250 °C).

The thin film RTD sensor used in this work was made of nickel due to its high thermal coefficient and excellent resistance linearity in the range of bio-chemical reactions (−10 to 150 °C). Shadow masking was used to pattern

a 35 nm thick nickel film by thermal evaporation. The nickel evaporation process is also simple and inexpensive. To increase the device sensitivity to temperature changes from the reaction, the RTD surface area was larger than the chemical reaction area to ensure all the heat generated or absorbed was received by the RTD. A Keithley 2600 source/meter with 4-point configuration was used to measure the resistance change of the RTD caused by the temperature change from the bio-chemical reactions. The 4-point measurement setup was used to eliminate the effect of junction resistance and thermal fluctuations of electrical leads on the resistance measurement of the RTD sensor. The measurements, data acquisition and data-preprocessing were automated and controlled by a LabView™ program.

A bias current of 1 mA was applied using the Keithley 2600 source/meter to the RTD (1.1 kΩ) and the voltage drop across the RTD was measured to monitor the resistance change of the RTD. For the design shown in Fig. 1, the 1 mA sourcing current through the RTD resulted in 0.11 mW of Joule heating, which elevated the RTD temperature approximately 1–2 °C above the room temperature. The resistance value of the RTD can be written as

(8) $R = R_0(1 + \alpha\Delta T)$

where R_0 is the resistance of the RTD at room temperature, α is the temperature coefficient of resistance and ΔT is the temperature change.

The thin film nickel RTD was calibrated using a thermal bath (HAAKE) to get the thermal coefficient of resistance (TCR). The nickel RTD showed a linear response between 10 °C and 50 °C ($R^2 = 0.9999$). The TCR of the nickel RTD was measured to be 0.0011/K, which was lower than values reported for bulk nickel ($6.14\times10^{-3}/K$) (Lacy, 2011). Since α is a function of the ratio of film thickness to the mean free path of electrons in metals (Jin et al., 2008, Leonard and Ramey, 1966), the difference is likely due to the film thickness (35 nm) and grain size of the thermally evaporated thin nickel film. Increasing the film thickness and a post-annealing process would likely improve the TCR.

3. Results

In order to demonstrate that the paper-based microcalorimetric detection method works, three applications were investigated: detection of glucose, detection of DNA, and the detection of streptavidin and biotin binding.

3.1. Glucose detection

The concentration of glucose was measured using the heat generated by the glucose oxidase (GOD) enzyme, which was used to convert glucose to gluconic acid and hydrogen peroxide. Due to its low pH sensitivity, GOD from *Aspergillus niger* (SigmaAldrich-G7141) was used to prepare a 1.0 mg/ml reagent in a 50 mM sodium acetate buffer. Sodium acetate buffer, as well as sodium phosphate buffer, is commonly used to activate GOD enzymes (Gibson et al., 1964). The buffer was made from anhydrous sodium acetate (Fisher Scientific-S210-2) and diluted with acetic acid to maintain the pH of the buffer constantly at 5.1. The activated GOD enzyme in the buffer was used to react with different concentrations of glucose. The GOD enzyme catalyzes the oxidation reaction of glucose (Bankar et al., 2009),

(9) $\beta DGlucose + O_2 \overset{GOD}{\rightarrow} \beta DGlucono - \delta lactone + H_2O_2$

This reaction causes an enthalpy change of $\Delta H = -80\mathrm{kJ/mol}$ (Scheper, 1999). Two microliters of active GOD enzyme were placed and immobilized at the reagent introduction site of the paper strip as shown in Fig. 1(a) and (b). The heat generated by the oxidation of glucose was recorded for different concentrations of glucose samples introduced to the immobilized GOD. Measurements for each concentration were repeated 10 times to calculate the measurement error. The measurement for each sample concentration was a temperature–time

plot which was post-processed to extract the temperature change for each sample concentration. Commercially available glucose solutions were used to test three different concentrations of glucose which were representative of low, normal and high glucose levels in the blood (0.05, 0.12 and 0.3% wt/vol of glucose, respectively) (Bayer Contour Control Solution) (Frank et al., 2011, Kilo et al., 2005). Fig. 2 shows a typical temperature profile from the reaction.

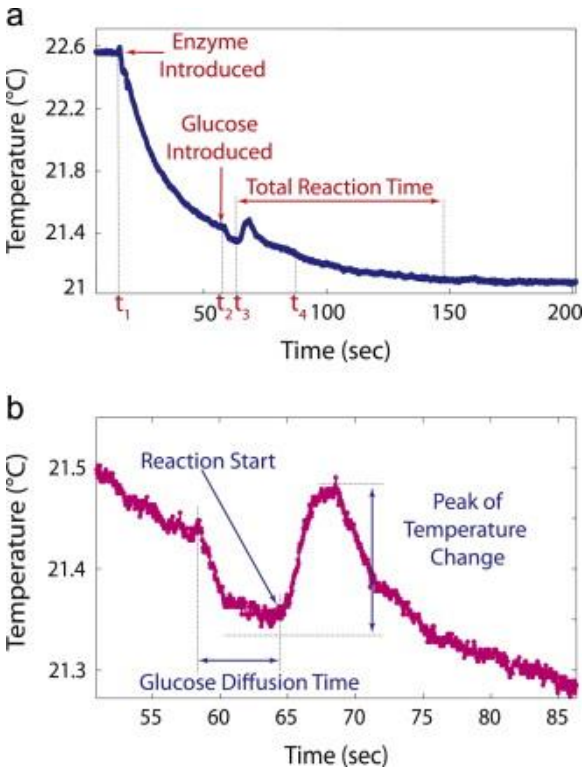

Fig. 2. Measured temperature change for reaction of glucose oxidase enzyme and glucose sample is illustrated. (a) Measured reaction data, (b) close-up reaction data from t_1 to t_4.

When the 2µL volume of GOD enzyme was first placed at t_1 (in Fig. 2) at the center of the paper strip, the temperature of the RTD dropped due to the temperature difference between the RTD and GOD enzyme and evaporative cooling of the enzyme buffer. The time between t_1 and t_2 shows the aforementioned temperature drop. The temperature of the RTD and the enzyme reached a stable temperature, which was still higher than room temperature because the RTD Joule heating. After the temperature was stabilized, an 8µL glucose sample at room temperature was placed to the tail of the L-shaped paper strip (sample inlet shown in Fig. 1), and traveled along the strip toward the GOD enzyme. During the time period between t_2 and t_3, the glucose continued to travel along the paper strip before it reached the enzyme site. The temperature drop during this period is again due to a temperature difference between the RTD and the glucose, and the evaporation of the sample. At time t_3, before the reaction, the glucose sample reached the enzyme and the oxidation reaction of glucose commenced. Due to the exothermic nature of the glucose oxidation process, the temperature rises. As the reaction completed, the temperature decreased, and reached equilibrium with surroundings.

The following equation is used to correlate the peak of temperature change, ΔT, to the concentration of glucose (Scheper, 1999)

(10) $n_p = C_p \frac{\Delta T}{\Delta H}$

where ΔH is molar enthalpy change, n_p is moles of product, and C_p is the heat capacity of the system.

The heat capacity (or thermal mass) of the system is calculated by calibrating with a low concentration of the glucose test sample. Knowing the exact concentration of glucose, enthalpy change, and temperature change, the thermal mass of our system can be determined. The effect of sample evaporation is also taken into account in the calibration.

The detected temperature for different concentrations of glucose shows an upward trend with increasing concentration as shown in Fig. 3. In order to convert the detected temperature to concentration data using Eq. (10), two additional terms must be considered: the reaction rate of GOD and glucose, and the ratio of reaction area to the total RTD area. For the reaction rate of GOD and glucose, the catalytic reaction of the enzyme can be saturated and shows a nonlinear behavior as the concentration of the glucose increases because the finite reaction rate is limited by the number of available GOD oxidation sites for glucose molecules (the Michaelis–Menten model for enzyme kinetics Murugan, 2002). In this experiment the number of moles of glucose is calculated by the concentration and the volume size of the samples. In the 8μL droplets of the low, normal, and high concentrations of the glucose test sample, a total number of 1.34×10^{16}, 3.21×10^{16} and 8.02×10^{16} molecules of glucose are available to react with the GOD, respectively. The calculated number of molecules of glucose in the sample is higher than the number of the molecules of the GOD, which is 7.53×10^{15} molecules in 2μL of enzyme. Therefore, the reaction is in the saturated region of the reaction rate. However, at high concentrations the reaction rate can be modeled as linear (Pant et al., 2008). For the ratio of reaction area to the total RTD area, the reaction area is designed to be 45% of the whole channel area. Therefore only 4μL of glucose is reacting with GOD.

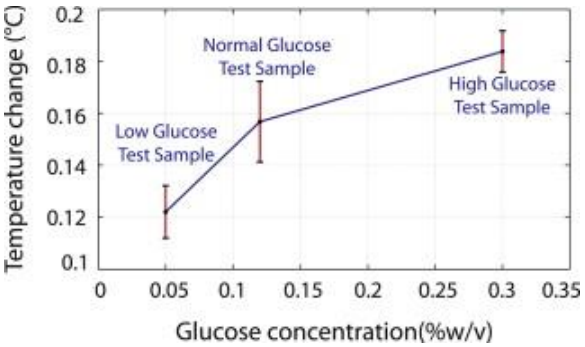

Fig. 3. Measured temperature change for different concentrations of glucose. Error bars are standard deviation of the samples where 10 different measurements for each concentration are performed.

Fig. 4 shows the measured glucose concentrations of the glucose test solution, taking the reaction rate factor and the ratio of reaction area into account. The results are also affected by the diffusion time of glucose into the GOD reaction site and the error may be resolved with optimizing the paper channel design. Results show good linearity and agreement with the solution concentrations from the manufacturer in the micro-molar range of glucose concentration. While a commercial glucose meter shows as high as 30% error in the glucose concentration measurement, the calorimetric paper-based microfluidic device shows less than 2% error as shown in Fig. 4.

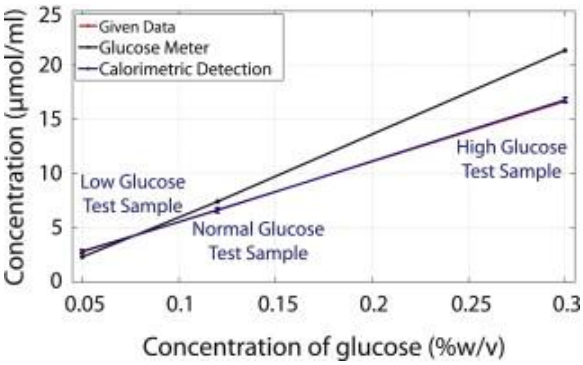

Fig. 4. The results of glucose with the paper-based calorimetric device and commercialized glucose meter for different concentrations.

Enzyme-based sensors have shown their expanding capabilities to improve health care quality. The integration of the paper-based technology and enzyme-based sensors may replace expensive and time consuming portions of clinical monitoring used by patient bedsides and home testing (Ispas et al., 2012). From Eq. (10), the detectable concentration is directly proportional to the temperature change, given the device heat capacity and enthalpy. Therefore, the concentration detection limit is determined by the minimum detectable temperature. With our measurement setup, the Kiethley 2600 source/meter, noise in the resistance is 0.004 Ω. The signal-to-noise ratio of 1:1 corresponds to 26 mK. With the signal-to-noise ratio, the measurable minimum concentration is 1.51µmole/mL.

3.2. DNA concentration detection

In biological systems, intracellular iron from ferritin reacts with hydrogen peroxide and catalyzes the formation of hydroxyl groups, which cleaves deoxyribonucleic acid (DNA) (Arosio and Levi, 2002). The reaction of the hydroxyl group and DNA causes DNA strand breakage (Mello-Filho et al., 1984). Hydrogen peroxide is a good source of hydroxyl groups, and is used in this work to react with salmon DNA in a buffer solution. The heat generated by the reaction was detected for different concentrations of salmon DNA (without the use of any catalyst). Deoxyribonucleic acid sodium salt from salmon testes (Sigma D1626) was used as the test DNA sample. DNA samples were diluted in IDTE DNA buffer (1xTE-pH8) to maintain the pH, and 30% wt/wt hydrogen peroxide solution (Fisher Scientific H325) was used for DNA detection experiments. The different concentrations of DNA reagents were placed to the reagent site on the paper microfluidic device, and then the hydrogen peroxide solution was introduced to the sample inlet on the channel. The hydrogen peroxide solution traveled along the paper and the reaction started when it reached the DNA sample location. The generated heat, proportional to the DNA concentration, was detected by the thin film RTD under the paper microfluidic device. To compare the results for different concentrations, four different reagents with different DNA concentrations were prepared (0.91 mg/ml, 1.83 mg/ml, 3.65 mg/ml, and 7.30 mg/ml). The generated heat by DNA experiments has the same pattern as the glucose detection experiment. The detected temperature change for different concentrations of DNA shows a rising trend as the concentration goes up. As shown in Fig. 5, a higher concentration caused a higher temperature change. Differential measurement (Fig. 5(a) and (b)) was used to minimize the effect of buffer on temperature measurement.

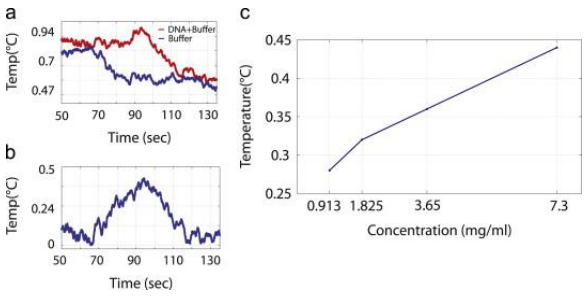

Fig. 5. The DNA concentration detection experiment results. (a) Signals from control experiments, a peak in temperature at the presence of DNA shows the oxidation reaction, (b) differential signal which shows the temperature change only from DNA reaction, (c) measured temperature change from the reaction of different DNA concentrations and hydrogen peroxide.

The main point of this experiment is to demonstrate low-cost DNA concentration detection. The purification of DNA after extraction is necessary for many sequencing approaches. Therefore, this method provides a low cost and simple way to monitor the concentration of DNA.

3.3. Protein binding detection

Protein–protein binding is used to identify or isolate different kinds of cells with related biomarkers, as well as in disease detection by studying the reaction of antibodies and antigens. Microfluidic devices have been developed for the detection of the protein binding via calorimetry (Torres et al., 2004). Biotin and streptavidin binding was selected to demonstrate the paper-based calorimeter device for an enthalpy assay. The biotin was placed at the reagent introduction site of the paper strip and the streptavidin was introduced to the sample inlet. The streptavidin travels along the paper to the biotin while the temperature was continuously recorded. Biotin (Sigma B4501) and streptavidin (Sigma S4762) are both diluted in DI water to prepare 1 mg/ml and 0.1 mg/ml solutions, respectively. Detection of protein binding is identified by the temperature spike in the temperature–time recording, resulting in a label-free detection mechanism (Ray et al., 2010).

For the binding of the proteins, the 2µL of diluted biotin is placed first on the strip. Again as in the glucose and DNA cases, this causes the temperature drops due to the temperature difference and evaporative cooling. By introducing the 5µL of streptavidin to the sample inlet, streptavidin is transported to the reagent and as soon as it gets to the biotin, a temperature change is detected. The temperature signal has the same pattern as previous experiments, which makes it possible to extract sample concentration by applying the same approaches. Fig. 6 illustrates the binding detection based on the enthalpy change with the paper-based microfluidic device. This result shows the feasibility of the device for thermal detection of protein binding events.

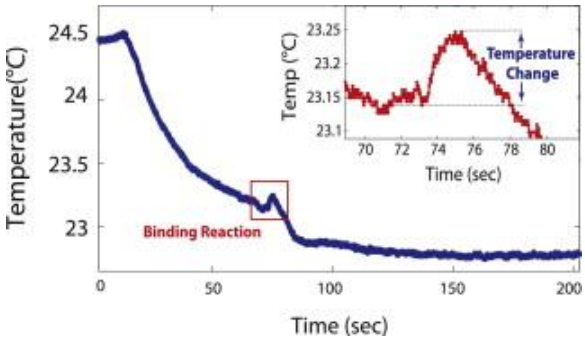

Fig. 6. Measured temperature change for binding reaction of biotin and streptavidin.

4. Discussion

The ultimate detection limit of the paper-based calorimetric device will be determined by the noise of the detection system. The calculated Johnson noise floor of the sensor RTD is 40 μΩ with a measurement bandwidth of 100 Hz. However, the lower limit of detection was determined by the Source/Meter, which had a resolution of 1mΩ. Experiments showed that the system was capable of reliably measuring changes in resistance as low as 4mΩ (26 mK) of 1.1kΩ. Because the temperature of the RTD is a function of the TCR (α), improving purity (in our evaporated nickel film case) or using a material with higher α will directly improve the measurement sensitivity.

The knife plotter cut paper strips used in this work can be further optimized to effectively guide the reactants (reagent and sample). The paper microfluidic channel design with only the knife plotter cut induces the flow of reactants when mixed, which contributed to the measurement of errors in Fig. 3. Also, the glucose diffusion time to reach the GOD is solely limited by the length of the strip. Combining techniques such as wax patterning and surface treatments along with improved cutting can significantly improve the reactant transport stability resulting in better measurement repeatability. In Fig. 6, the temperature profiles before and after the reaction varied due to evaporation of liquid to surroundings. In the ideal case, the temperature profile should follow a monotonic decrease. The deviation prevents accurate calculation of the area under the reaction, which may be used for calculation of total enthalpy of the reaction. This deviation can be minimized by optimizing the paper strips.

The calorimetric detection mechanism is a label-free method that allows the expansion of applications of enzyme-based sensors to a wide range of enzymatic reactions. The application of this type of portable device has been limited due to the complexity of detection methods. The calorimetric method overcomes these limitations and could result in new devices with applications in portable healthcare diagnostics. Calorimetric DNA concentration detection is a method in which thermal information from the reaction can be used to obtain useful information about DNA. Calorimetric protein binding detection using the paper-based micro-calorimetric device has the ability to expand the applications of current disposable disease detection devices. The calorimetric detection demonstrated in this paper can expand the functionality of microanalytical devices by adding a thermal detection scheme for bio-chemical materials based on the enthalpy changes.

5. Conclusion

A framework for using calorimetric detection with paper-based analytical devices is presented. The calorimetric detection method of the reaction on a paper network is a novel technique that expands the detection capabilities of paper-based sensors. The paper-based calorimetric method is capable of detecting various enzymatic and biological reactions with an electronic readout. Calorimetric detection for three different bio-chemical samples is demonstrated. The results demonstrate the feasibility of the calorimetric paper-based device to detect various bio-chemical reactions without having any embedded markers or complex measurements. The thermal detection paper-based analytical device will help realize future low-cost, portable, and non-complex point-of-care devices.

Acknowledgments

We thank Glenn M. Walker and Shankar Radhakrishnan for helpful discussions.

References

Abramson and Tien, 1999. A.R. Abramson, C.L. Tien. *Microscale Thermophys. Eng.,* 3 (4) (1999), pp. 229-244
Allen and Lai, 1998. L.H. Allen, S.L. Lai. *Microscale Thermophys*. Eng., 2 (1) (1998), pp. 11-19
Arosio and Levi, 2002. P. Arosio, S. Levi. *Free Radic. Biol. Med*., 33 (4) (2002), pp. 457-463

Bankar et al., 2009. S.B. Bankar, M.V. Bule, R.S. Singhal, L. Ananthanarayan. *Biotechnol. Adv*., 27 (4) (2009), pp. 489-501

Barnes et al., 1994.
J.R. Barnes, R.J. Stephenson, C.N. Woodburn, S.J. O'Shea, M.E. Welland, T. Rayment, J.K. Gimzewski, C. G erber. *Rev. Sci. Instrum*., 65 (12) (1994), pp. 3793-3798

Bergman et al., 2011. T.L. Bergman, A.S. Lavine, F.P. Incropera, D.P. DeWitt. *Foundamental of Heat and Mass Transfer.* (seventh edition.), John Wiley and Sons Inc., United States. (2011)

Carrilho et al., 2009. E. Carrilho, A.W. Martinez, G.M. Whitesides. *Anal. Chem*., 81 (16) (2009), pp. 7091-7095

Carslaw and Jaeger, 1986. H.S. Carslaw, J.C. Jaeger. *Conduction of Heat in Solids.* Oxford University Press, Oxford (1986)

Cho et al., 2007. C.-H. Cho, W. Cho, Y. Ahn, S.-Y. Hwang. *J. Micromech. Microeng*., 17 (9) (2007), p. 1810

Dungchai et al., 2011. W. Dungchai, O. Chailapakul, C.S. Henry. *Analyst*, 136 (2011), pp. 77-82

Ellerbee et al., 2009.
A.K. Ellerbee, S.T. Phillips, A.C. Siegel, K.A. Mirica, A.W. Martinez, P. Striehl, N. Jain, M. Prentiss, G.M. Wh itesides. *Anal. Chem*., 81 (20) (2009), pp. 8447-8452

Frank et al., 2011 J. Frank, J.F. Wallace, S. Pardo, J.L. Parkes. *J. Diabetes Sci. Technol*., 5 (1) (2011), pp. 198-205

Fu et al., 2011. E. Fu, S. Ramsey, P. Kauffman, B. Lutz, P. Yager. *Microfluid. Nanofluidics*, 10 (1) (2011), pp. 29-35

Gibson et al., 1964. Q.H. Gibson, B.E.P. Swoboda, V. Massey. *J. Biol. Chem*., 239 (11) (1964), pp. 3927-3934

Ispas et al., 2012. C.R. Ispas, G. Crivat, S. Andreescu. *Anal. Lett*., 45 (2–3) (2012), pp. 168-186

Jin et al., 2008. J.S. Jin, J.S. Lee, O. Kwon. *Appl. Phys. Lett*., 92 (17) (2008)

Kilo et al., 2005. C. Kilo, M. Pinson, J.O. Joynes, H. Joseph, N. Monhaut, J.L. Parkes, J. Baum. *Diabetes Technol. Ther*., 7 (2) (2005), pp. 283-294

Kwak et al., 2008. B.S. Kwak, H.O. Kim, J.H. Kim, S. Lee, H.-I. Jung. *Biosens. Bioelectron*., 10 (1) (2008), pp. S10-S26

Lacy, 2011. F. Lacy. *IEEE Sens. J.,* 11 (5) (2011), pp. 1208-1213

Lai et al., 1995. S.L. Lai, G. Ramanath, L.H. Allen, P. Infante, Z. Ma. *Appl. Phys. Lett*., 67 (9) (1995), pp. 1229-1231

Leonard and Ramey, 1966. W.F. Leonard, R.L. Ramey. *J. Appl. Phys*., 37 (9) (1966)

Li et al., 2012. X. Li, D.R. Ballerini, W. Shen. *Biomicrofluidics*, 6 (1) (2012)

Liana et al., 2012. D.D. Liana, B. Raguse, J.J. Gooding, E. Chow. *Sensors*, 12 (9) (2012), pp. 11505-11526

Liu and Crooks, 2011. H. Liu, R.M. Crooks. *J. Am. Chem. Soc*., 133 (44) (2011), pp. 17564-17566

Martin, 1952. Martin, A., 1952. *The development of partition chromatographys*. Nobel Lecture.

Martinez et al., 2007. A.W. Martinez, S.T. Phillips, M.J. Butte, G. Whitesides. *Angew. Chem. Int. Ed*., 46 (8) (2007), pp. 1318-1320

Martinez et al., 2008a. A.W. Martinez, S.T. Phillips, E. Carrilho, S.W. Thomas, H. Sindi, G.M. Whitesides. *Anal. Chem*., 80 (10) (2008), pp. 3699-3707

Martinez et al., 2008b. A.W. Martinez, S.T. Phillips, B.J. Wiley, M. Gupta, G.M. Whitesides. *Lab Chip*, 8 (2008), pp. 2146-2150

Mello-Filho et al., 1984. A.C. Mello-Filho, M.E. Hoffmann, R. Meneghini. *Biochem. J.,* 218 (1) (1984). 273-0

Muller and Clegg, 1949. R.H. Muller, D.L. Clegg. *Anal. Chem*., 21 (9) (1949), pp. 1123-1125

Murugan, 2002. R. Murugan. *J. Chem. Phys*., 117 (9) (2002)

Nie et al., 2010.
Z. Nie, C.A. Nijhuis, J. Gong, X. Chen, A. Kumachev, A.W. Martinez, M. Narovlyansky, G.M. Whitesides. *Lab Chip*, 10 (2010), pp. 477-483

Pant et al., 2008. M. Pant, P. Sharma, T. Radha, R. Sangwan, U. Roy. *J. Biol. Sci.,* 8 (8) (2008), pp. 1322-1327

Ray et al., 2010. S. Ray, G. Mehta, S. Srivastava. *Proteomics*, 10 (4) (2010), pp. 731-748

Scheper, 1999. Scheper, T., 1999. Advances in Biochemical Engineering/Biotechnology, Thermal Biosensors Bioactivity *Bioaffinity*, vol. 64. Springer-Verlag, Berlin, Heidelberg.

Sung and Shuler, 2009. J.H. Sung, M.L. Shuler. *Biomed. Microdev*., 11 (4) (2009), pp. 731-738

Torres et al., 2004. F.E. Torres, P. Kuhn, D. De
Bruyker, A.G. Bell, M.V. Wolkin, E. Peeters, J.R. Williamson, G.B. Anderson, G.P. Schmitz, M.I. Recht, S. Sc

hweizer, L.G. Scott, J.H. Ho, S.A. Elrod, P.G. Schultz, R.A. Lerner, R.H. Bruce. *Proc. Natl. Acad. Sci. U. S. A.,* 101 (26) (2004), pp. 9517-9522

Wang, 2008. J. Wang. *Chem. Rev*., 108 (2) (2008), pp. 814-825

Yi et al., 2014. C. Yi, J.-H. Lee, B.S. Kwak, M.X. Lin, H.O. Kim, H.-I. Jung. *Sens. Actuators B: Chem*., 191 (0) (2014), pp. 305-312